PERGAMON

International Journal of Multiphase Flow 27 (2001) 217–236

International Journal of Multiphase Flow

www.elsevier.com/locate/ijmulflow

Temporal properties of secondary drop breakup in the multimode breakup regime

Z. Dai, G.M. Faeth*

Department of Aerospace Engineering, The University of Michigan, Ann Arbor, MI 48109-2140, USA

Received 7 July 1999; received in revised form 6 February 2000

Abstract

Secondary drop breakup due to shock wave disturbances was studied for the multimode breakup regime, emphasizing the temporal evolution of breakup for shock wave disturbances. Measurements were carried out in a shock tube using pulsed shadowgraphy and holography to observe the mechanism and outcome of breakup. Test conditions involved water and ethanol drops, liquid/gas density ratios greater than 500, Ohnesorge numbers less than 0.1 and Weber numbers of 15–150. The evolution of properties in the multimode breakup regime with increasing Weber number begins at the end of the bag breakup regime with the appearance of a plume drop at the apex of the bag at a Weber number of roughly 15, continues in a bag/plume breakup regime which involves the presence of both bag-like structures and plume drops and transitions when bags are no longer present at a Weber number of roughly 40, and ends with a plume/shear breakup regime which involves development of plume-like structures that progressively evolve into a parent drop and ligament system as the shear breakup regime is approached at a Weber number of roughly 80. Measurements over the test range provide breakup times, drop deformation properties and drag coefficients before the onset of breakup, distributions of drop liquid and resulting drop sizes for various breakup structures, drop velocities after breakup, and liquid removal rates during breakup; all these properties are provided as a function of Weber number in the multimode breakup regime.

Keywords: Drop breakup; Drop dynamics; Pulsed holography; Sprays; Atomization

* Corresponding author. Tel.: +1-734-764-7202; fax: +1-734-936-0106.
E-mail address: gmfaeth@umich.edu (G.M. Faeth).

0301-9322/01/$ - see front matter
PII: S0301-9322(00)00015-X

1. Introduction

The secondary breakup of drops is an important fundamental process of sprays. For example, drops formed by primary breakup are intrinsically unstable to secondary breakup whereas secondary breakup can be the rate controlling process within dense sprays in much the same way as drop vaporization can be the rate controlling process within dilute sprays (Faeth, 1990; Wu et al., 1995). Motivated by these observations, Chou et al. (1997) and Chou and Faeth (1998) extended earlier studies of the regimes and outcomes of secondary breakup caused by shock-wave disturbances due to Hsiang and Faeth (1992, 1993, 1995) to consider the properties and the formation rates of drops resulting from secondary breakup as a function of time in the bag and shear breakup regimes. The present study seeks to extend this work to the more complex multimode breakup regime that is bounded by these regimes.

Earlier studies of secondary breakup are discussed by Giffen and Muraszew (1953), Hinze (1955), Clift et al. (1978), Krzeczkowski (1980), Wierzba and Takayama (1987, 1988), Faeth (1990), Wu et al. (1995) and Gel'fand (1996), among others. Shock-wave disturbances were considered during most earlier studies, providing a step change of the drop environment, similar to conditions experienced by drops at the end of primary breakup. The main findings of early works included the conditions required for particular deformation and breakup regimes, time required for the onset and end of primary breakup, the drag properties of deformed drops in the period before breakup begins, and the drop size and velocity distributions that resulted from the breakup process (i.e., the jump conditions). This behavior can be illustrated in terms of the characteristic shear breakup time of Ranger and Nicholls (1969), t^*, defined as follows:

$$t* = d_0\left(\rho_L/\rho_G\right)^{1/2}/u_0 \tag{1}$$

In Eq. (1) d_0 and u_0 are the initial drop diameter and relative velocity, ρ denotes density, and the subscripts L and G denote liquid and gas properties, respectively. Liang et al. (1988) show that the average breakup time for a wide range of drop conditions is roughly $5.5t*$, which is comparable to flow residence times within the dense spray region where secondary breakup is a dominant process (Faeth, 1990; Wu et al., 1995). Put another way, the original (or parent) drop moves roughly $50d_0$ and the smallest drops formed by secondary breakup move roughly $100d_0$ during the breakup time for typical shear breakup processes (Hsiang and Faeth, 1993, 1995) which can be a significant fraction of the dense spray region. This implies that secondary breakup should be treated as a rate process rather than by jump conditions in some instances. Work to provide the temporal properties of breakup in the bag and shear breakup regimes for drop breakup in gases at standard temperature and pressure (STP), and for conditions where effects of liquid viscosity are small, was completed by Chou et al. (1997) and Chou and Faeth (1998). The present investigation continues the study of the temporal properties of secondary breakup when effects of liquid viscosity are small, by considering the multimode breakup regime. The objective is to provide a way to estimate the temporal properties of secondary drop breakup that can be used within contemporary models of sprays, see Faeth (1990, 1996) and references cited therein for descriptions of typical spray models.

The present measurements were carried out using a shock tube facility with the drop

environment during secondary breakup approximating air at STP. Single- and double-pulse shadowgraphy and holography were used to find the degree of deformation and drag coefficients prior to the onset of breakup, the size and velocity properties of drops produced by secondary breakup and the rate of liquid removal from the parent drop as a function of time. Multimode breakup is more complex than the bag and shear breakup regimes; therefore, visualization of breakup within this regime was emphasized in order to establish subregimes involving particular breakup mechanisms. Finally, earlier information about the onset and end of multimode breakup was limited so that additional measurements of this type were carried out as well. Similar to the earlier studies of the temporal properties of bag and shear breakup regimes (Chou et al., 1997; Chou and Faeth, 1998), test conditions were most representative of drop breakup within sprays having modest liquid viscosities at STP.

2. Experimental methods

2.1. Apparatus and instrumentation

The test apparatus and instrumentation will be described only briefly because it was similar to earlier work (Hsiang and Faeth, 1992, 1993, 1995; Chou et al., 1997; Chou and Faeth, 1998). The tests were carried out in a rectangular shock tube with the driven section open to the atmosphere and the side walls windowed to provide optical access. A vibrating capillary tube drop generator similar to Dabora (1967) and an electrostatic drop selection system similar to Sangiovanni and Kestin (1977) provided a stream of drops having sufficient spacing so that there was negligible drop–drop interactions within the multimode breakup regime.

Single- and double-pulse shadowgraphy and holography were used to visualize the secondary breakup process, and to measure the properties of the parent drop and the drops produced by secondary breakup as a function of time. Laser pulse times were only 7 ns, which stopped drop motion; a weaker second laser pulse allowed directional ambiguity to be resolved during velocity measurements. Objects as small as 6 μm could be observed and as small as 10 μm could be measured with 10% accuracy. Results at each test condition were averaged over no less than four realizations, considering 100–200 liquid elements, in order to find drop diameter and velocity properties. Estimated experimental uncertainties (95% confidence) are less than 15% for drop diameters and less than 20% for streamwise velocities.

2.2. Test conditions

The test conditions are summarized in Table 1. Liquid properties were obtained from Lange (1952). Parameters given in the table include the Weber number, $We = \rho_G u_0^2 d_0/\sigma$, the Reynolds number, $Re = \rho_G u_0 d_0/\mu_G$, and the Ohnesorge number, $Oh = \mu_L/(\rho_L d_0 \sigma)^{1/2}$ where σ is the surface tension and μ is the molecular viscosity. Earlier work has shown that dimensionless properties such as the Weber number, Ohnesorge number, density ratio, etc., provide an adequate treatment of different liquid properties for secondary breakup effects (Chou and Faeth, 1998; Chou et al., 1997; Hsiang and Faeth, 1992, 1993, 1995). As a result, only water and ethanol were used as the drop liquids in order to check effects of liquid properties. The

Weber number range was prescribed to cover the multimode breakup regime and to extend results to overlap portions of both the bag and shear breakup regimes. The Reynolds number range of the experiments is larger than the conditions where gas viscosity has a significant effect on drop drag properties, e.g., the drag coefficient, C_D, for spheres varies only in the range 0.4–0.5 for this Reynolds number range (White 1974). Shock wave Mach numbers were relatively small, less than 1.24; therefore, the physical properties of the gas surrounding the drops during breakup was nearly the same as air at STP.

3. Results and discussion

3.1. Flow visualization

Pulsed shadowgraphy flow visualization was used to help resolve the rich variation of behavior seen in the multimode breakup regime. Typical visualizations are presented in Figs. 1–7 for drops having $We = 15$, 20, 25, 32, 40, 50 and 81, respectively, with $Oh < 0.1$, which places these results at conditions where effects of liquid viscosity are negligible. Shadowgraphs are shown for each condition at various values of t/t^* during the breakup process, where t denotes time after the shock wave passes the drop. The shock wave and flow velocities behind the shock wave are directed from the top to the bottom of the shadowgraphs.

Fig. 1 is an illustration of typical shadowgraphs of behavior in the bag breakup regime with $We = 15$, as a baseline for behavior in the multimode breakup regime. Similar to the observations of Chou and Faeth (1998), various conditions during bag breakup can be defined as follows: the deformation period where the drop deforms from a spherical to a disk-like shape for $t/t^* = 0$–2.0, the bag growth period where the center of the disk deforms into a thin membrane-like bag with a much thicker basal ring surrounding its open (upstream) end for t/t^* of 2.0–3.0, the bag breakup period where the bag progressively breaks up from its closed

Table 1
Summary of test conditions[a]

Parameter	Range
Liquid	Water,[b] ethanol[c]
Initial drop diameter	0.50–0.80 mm
Liquid/gas density ratio (ρ_L/ρ_G)	680–850
Weber number (We)	15–150
Reynolds number (Re)	1500–3300
Ohnesorge number (Oh)	0.0045–0.013

[a] Air initially at 98.8 kPa and 298 ± 2 K in the driven section of the shock tube. Shock Mach numbers of 1.01–1.24. Properties of air taken at standard temperature and pressure: $\rho_G = 1.18$ kg/m^3, $\mu_G = 18.5 \times 10^{-4}$kg/ms.

[b] Properties of water taken at standard temperature and pressure: $\rho_L = 997$ kg/m^3, $\mu_L = 8.94 \times 10^{-4}$ kg/ms, $\sigma = 70.8$ mN/m.

[c] Properties of ethanol taken at standard temperature and pressure: : $\rho_L = 800$ kg/m^3, $\mu_L = 16.0 \times 10^{-4}$ kg/ms, $\sigma = 24.0$ mN/m.

downstream end toward the basal ring for t/t^* of 3.0–3.5, and the ring breakup period where a series of relatively large node drops form along the ring followed by breakup of the ring into a circular array of relatively large drops to end the breakup process for t/t^* of 3.5–4.5.

Fig. 2 shows typical pictures of breakup in a portion of the multimode regime, that will be called the bag/plume breakup regime, for a water drop having $We = 20$. Similar to $We = 15$, the drop deforms to disk-like shape for t/t^* of 0–2.0 and then the bag grows with the basal ring surrounding its open end. However, as the bag grows, a so-called plume drop also grows from the center of the bag; this plume drop can be seen clearly from the picture at $t/t^* = 2.7$. The plume drop is not connected to the basal ring. The existence of plume drop is characteristic of multimode (bag/plume) drop breakup. Measurements reveal that bag/plume breakup starts at roughly $We = 18$. At this condition, the bag breaks up from $t/t^* = 2.7$–3.5. The plume drop separates from the bag at $t/t^* = 3.0$ due to bag breakup. Also note that at $t/t^* = 3.5$, a large drop detaches from the plume drop, which will be called core drop. The basal ring breakup period is $t/t^* = 3.5$–3.8. Then the plume drop breaks up which ends the breakup process.

Fig. 3 shows typical pictures of multimode (bag/plume) breakup for a water drop having $We = 25$. Similar to $We = 20$, the drop deforms to a disk-like shape for $t/t^* = 0$–2.0. At $t/t^* = 2.3$, the bag, basal ring and plume drop can be seen clearly. However the sizes of the bag and

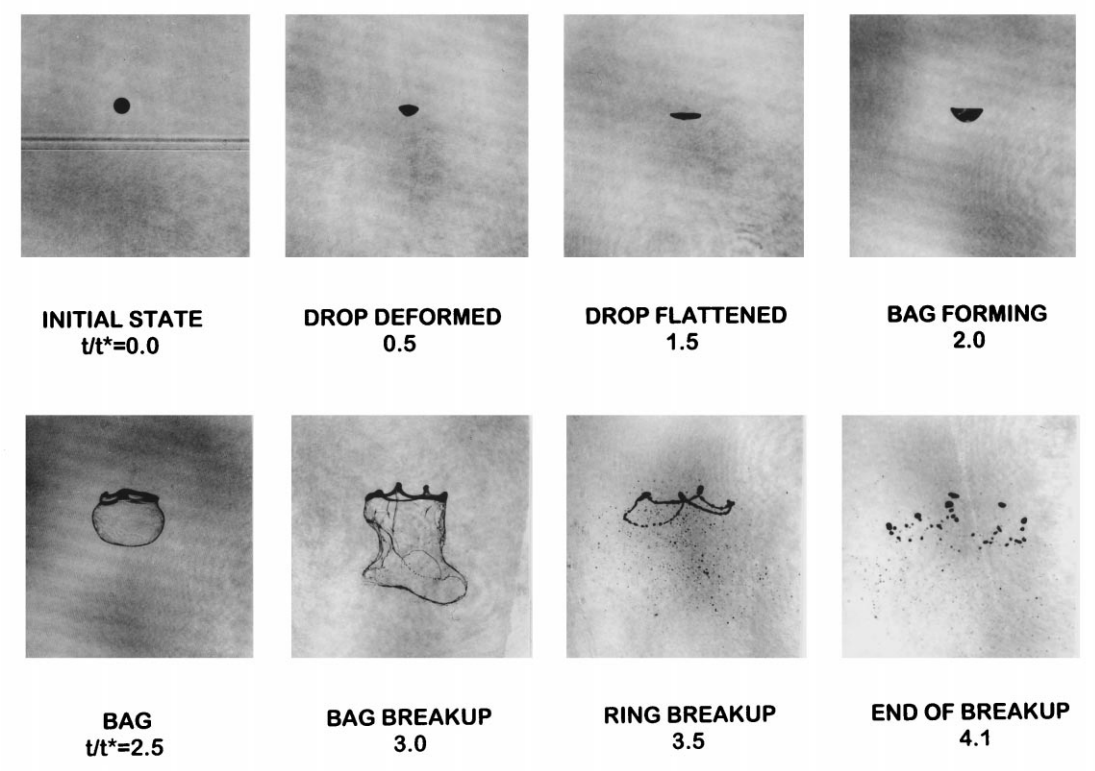

Fig. 1. Pulse shadowgraphs of secondary breakup in the bag breakup regime (water, $We = 15$, $Oh = 0.0045$).

basal ring are much smaller, while the size of plume drop has increased, compared to conditions seen in Fig. 2. The bag begins to break up at $t/t^* = 2.5$ and ends breakup before $t/t^* = 3.0$, which is sooner than observations at smaller We. The basal ring subsequently breaks up and leaves the plume drop at $t/t^* = 3.5$. The plume then undergoes Rayleigh breakup which is finished at $t/t^* = 5.7$. Note that the core drop forms at $t/t^* = 5.0$ and its shape is variable but more or less spherical.

Fig. 4 shows pictures of multimode (bag/plume) breakup at $We = 32$. The bag finishes breakup sooner than at smaller We, before $t/t^* = 2.3$. The ring and bag size continue to become smaller and the liquid volume inside the plume drop increases dramatically. The core drop forms after the plume finishes breakup, which is different from $We = 20$ and 25, where the core drop forms before the plume finishes breakup. The core drop is not spherical. Contrary to the expectation of deforming into a spherical core drop without any further breakup, the core drop undergoes Rayleigh breakup and finishes breakup at $t/t^* = 7.3$; therefore, the total breakup time is increased by roughly 60% compared to the breakup times in the bag and shear breakup regimes.

Fig. 5 shows pictures of breakup in a portion of the multimode regime, that will be called the plume/shear breakup regime, for a water drop having $We = 40$. At this condition, the bag

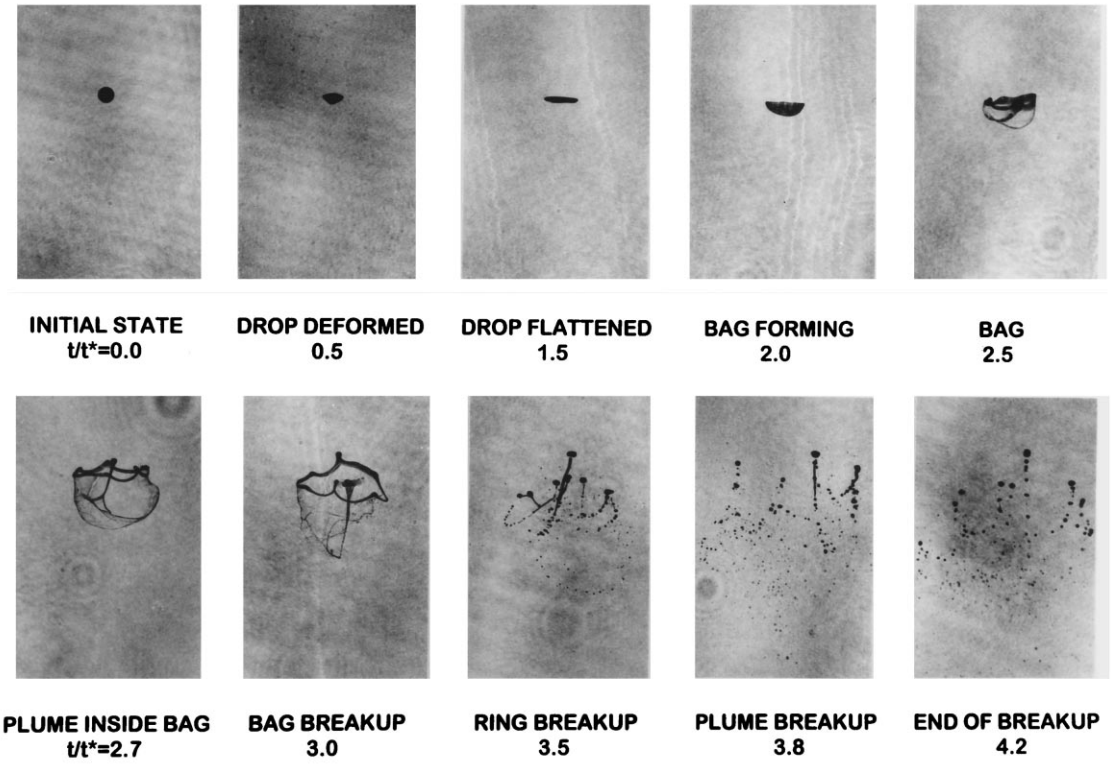

Fig. 2. Pulse shadowgraphs of secondary breakup in the bag/plume breakup regime (water, $We = 20$, $Oh = 0.0045$).

and ring do not appear any longer. The plume breakup process also differs from behavior at smaller We in the bag/plume breakup regime because the core drop does not detach from the plume; instead, the plume becomes simply an appendage of the core drop and drops are continuously removed from the core-drop/plume complex in a manner resembling the stripping mechanism of the shear breakup regime. Thus, while these conditions involve the presence of a plume, they have many of the characteristics of shear breakup, suggesting the plume/shear breakup regime designation. Finally, breakup of the core-drop/plume complex is relatively slow at this condition with the entire breakup process not complete until $t/t^* = 7.5$, which is the longest breakup time in the multimode breakup regime. This associated maximum breakup time, along with the disappearance of the bag and a detached plume, provide other reasons to designate the conditions of Fig. 5 as the onset of a new plume/shear breakup regime.

Fig. 6 shows typical pictures of multimode (plume/shear) breakup of a water drop having $We = 50$. The main difference between Figs. 5 and 6 as We increases in the plume/shear breakup regime is that the plume becomes less prominent. This trend continues with increasing We throughout the remainder of the plume/shear breakup regime. Another trend in this regime is a progressive reduction of t/t^* at the end of breakup with increasing We, as the size of the core-drop/plume complex continues to decrease.

Fig. 7 shows typical pictures at the onset of the shear breakup regime for an ethanol drop

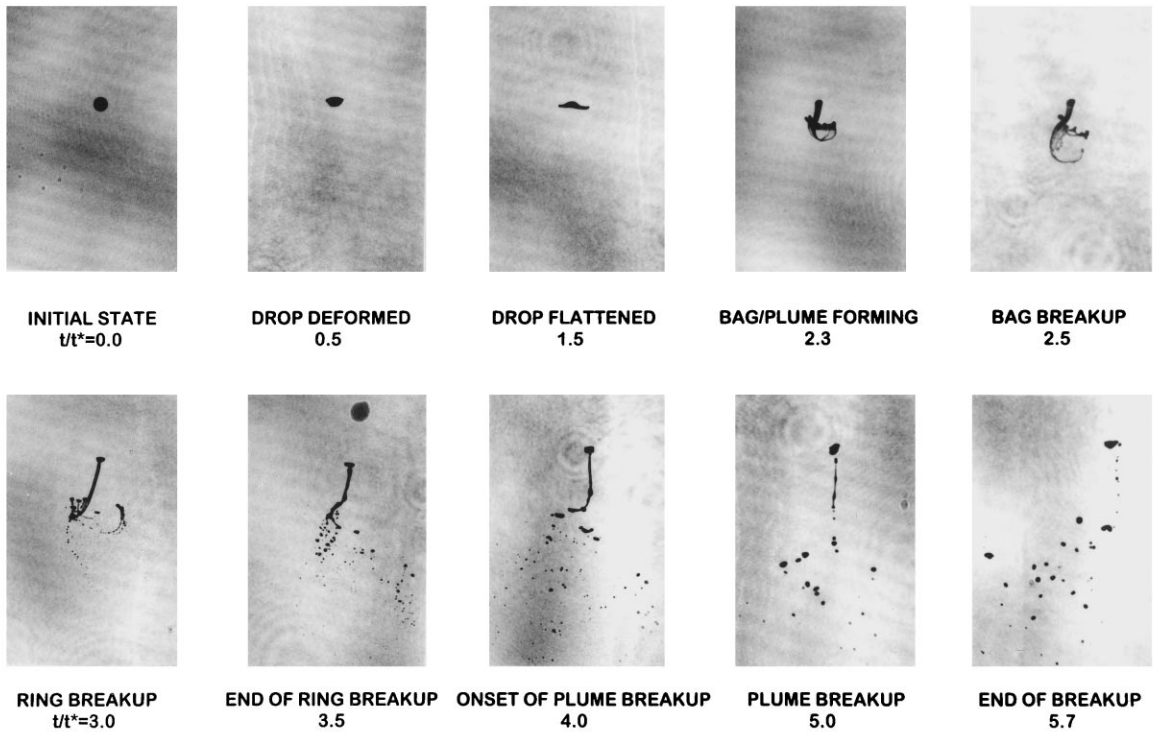

Fig. 3. Pulse shadowgraphs of secondary breakup in the bag/plume breakup regime (water, $We = 25$, $Oh = 0.0045$).

with $We = 80$. At this condition, a plume is no longer present with drops simply being stripped from the periphery of the flattened core drop. In addition, the increased breakup time due to the relatively slow breakup of the core-drop/plume complex has ended, and t/t^* has returned to values associated with the bag and shear breakup regimes, providing another reason to designate a transition to shear breakup at this condition.

3.2. Breakup times

Times of the onset and end of breakup are plotted as a function of We, for $Oh < 0.1$, in Fig. 8. These results include measurements of Hsiang and Faeth (1992), Chou et al. (1997), Chou and Faeth (1998) and the present investigation for $We = 15$–150, which spans the range from bag to well into the shear breakup regime. The breakup regimes that were described based on Figs. 1–7 are also marked on the plots with bag breakup observed for $We = 13$–18, multimode breakup for $We = 18$–80 and shear breakup for We greater than 80. In addition, the multimode breakup regime is divided into two subregimes as just discussed: bag/plume breakup for $We = 18$–40 and plume/shear breakup for $We = 40$–80. The agreement among the various measurements illustrated in Fig. 8 is seen to be very good.

The onset of breakup at small We in the bag breakup regime occurs for t/t^* of roughly 3.0.

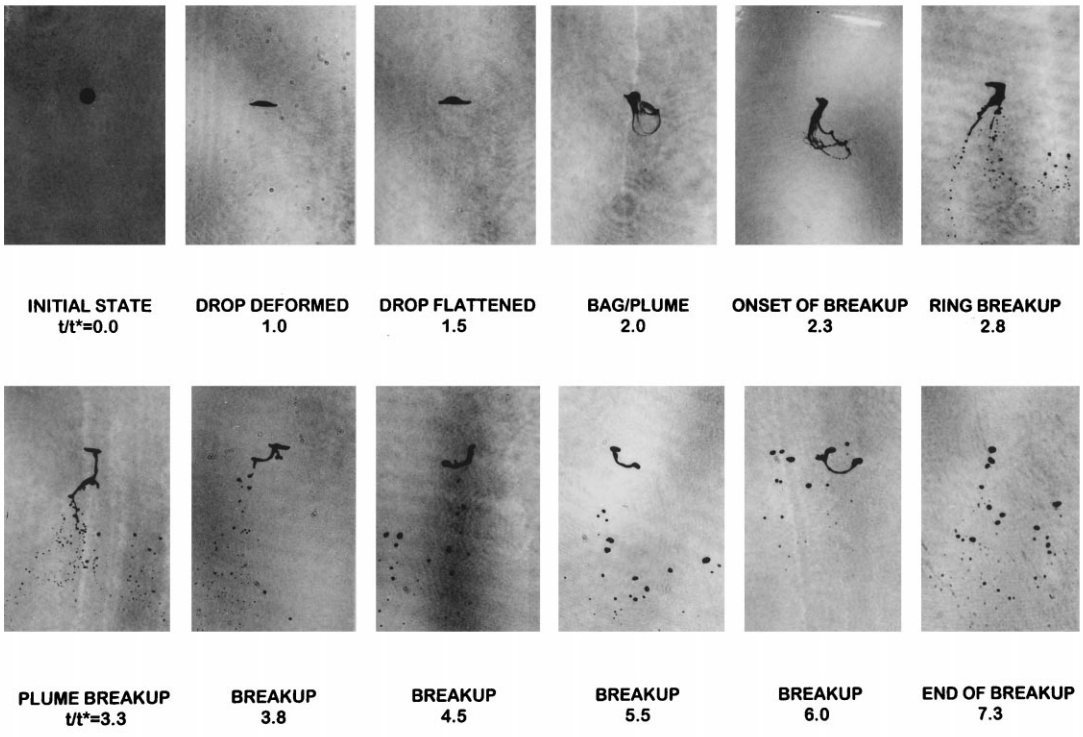

Fig. 4. Pulse shadowgraphs of secondary breakup in the bag/plume breakup regime (water, $We = 32$, $Oh = 0.0045$).

Onset times progressively decrease throughout the bag/plume breakup regime, however, before reaching values of $t/t^* = 2.0$ at larger values of We in the plume/shear and shear breakup regimes.

The end of breakup in the bag breakup regime occurs for t/t^* of roughly 4.0. Then, t/t^* at the end of breakup progressively increases with increasing We within the bag/plume breakup regime, reaching a maximum of t/t^* of roughly 7.5 at $We = 40$ where breakup makes the transition to the plume/shear breakup regime. Finally, t/t^* at the end of breakup progressively decreases with increasing We within the plume/shear breakup regime, reaching t/t^* at the end of breakup of roughly 5.0 at the onset of the shear breakup regime at $We = 80$. Hassler (1970) has reported similar behavior for the end of breakup over this Weber number range. It appears that the main reason for the local maximum of t/t^* at the end of breakup is the development of the large core-drop/plume complex and the relatively slow breakup of this complex by what appears to be a mainly relatively passive Rayleigh breakup process because the plume is sheltered to some extent by the core drop.

3.3. Drop deformation properties

The properties of drops in the period prior to the onset of breakup — drop deformation and drag coefficient properties — will be considered next. These properties are of interest because

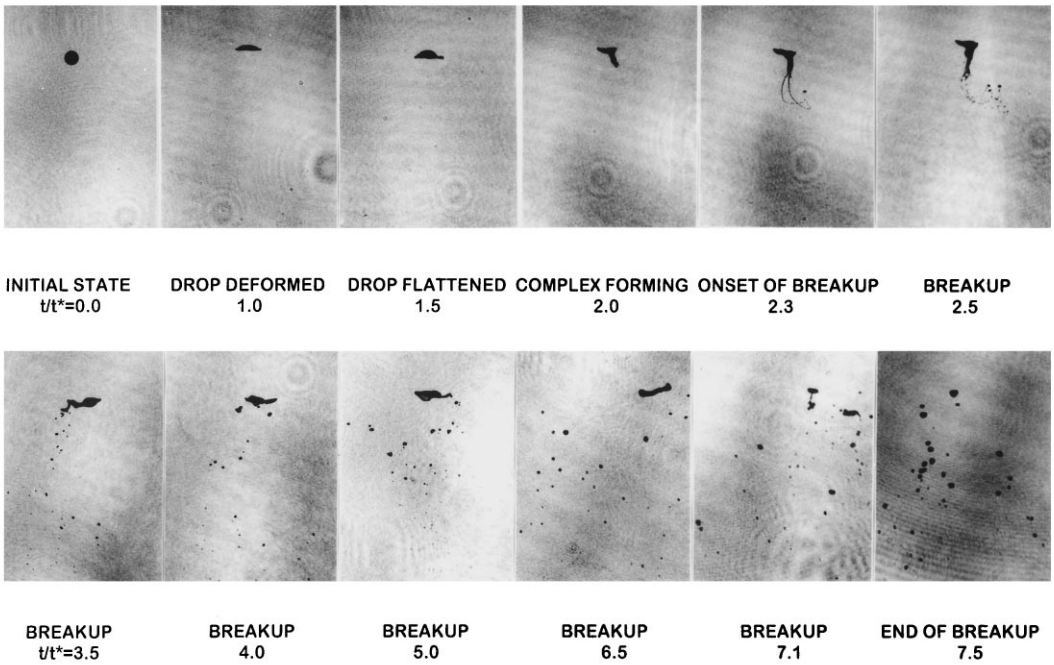

Fig. 5. Pulse shadowgraphs of secondary breakup in the plume/shear breakup regime (water, $We = 40$, $Oh = 0.0045$).

they can be used to evaluate numerical simulations of drop dynamics and as a crucial first step toward gaining a better understanding of secondary drop breakup.

Present measurements of maximum cross stream diameters of drops at the onset of secondary drop breakup, D_{Lmax}, are plotted as a function of the Weber number in Fig. 9. Earlier measurements of this property due to Hsiang and Faeth (1992) are also illustrated on the plot. Present measurements yield little variation of the maximum cross stream drop diameter as the Weber number is varied, yielding an average value of $D_{Lmax}/d_0 = 2.15$ in the multimode breakup regime. The results of Hsiang and Faeth (1992) agree with present measurements within experimental uncertainties but exhibit a consistent trend toward increasing D_{Lmax}/d_0 with increasing Weber number. Much of the increase in the Hsiang and Faeth (1992) correlation comes about, however, by fitting data extending from the bag breakup until well into shear breakup regime, e.g., $We < 100$.

The present measurements of the cross stream and streamwise dimensions of the deformed drop, D_{L} and D_{H}, are plotted as a function of normalized time, t/t^*, in Fig. 10. This plot is arranged as the normalized cross stream and streamwise distortions, $D_{\mathrm{L}} - d_0$ and $d_0 - D_{\mathrm{H}}$, as suggested by Hsiang and Faeth (1992). The correlation of cross stream distortion due to Hsiang and Faeth (1992) is also shown in the plot. This expression involves their measurements

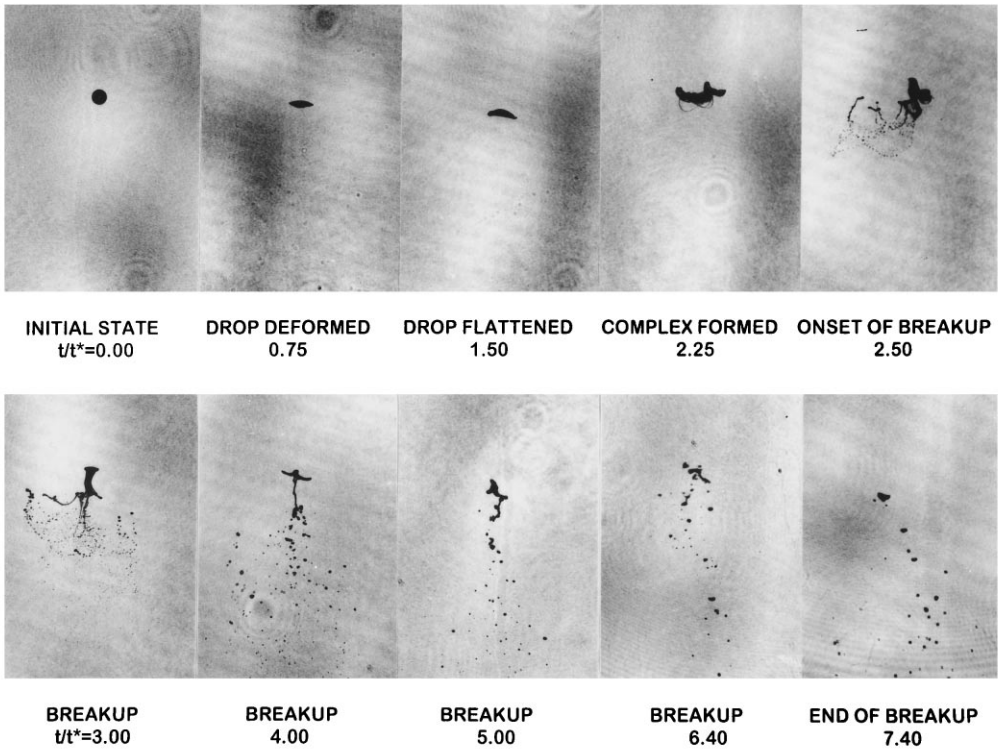

Fig. 6. Pulse shadowgraphs of secondary breakup in the plume/shear breakup regime (water, $We = 50$, $Oh = 0.0045$).

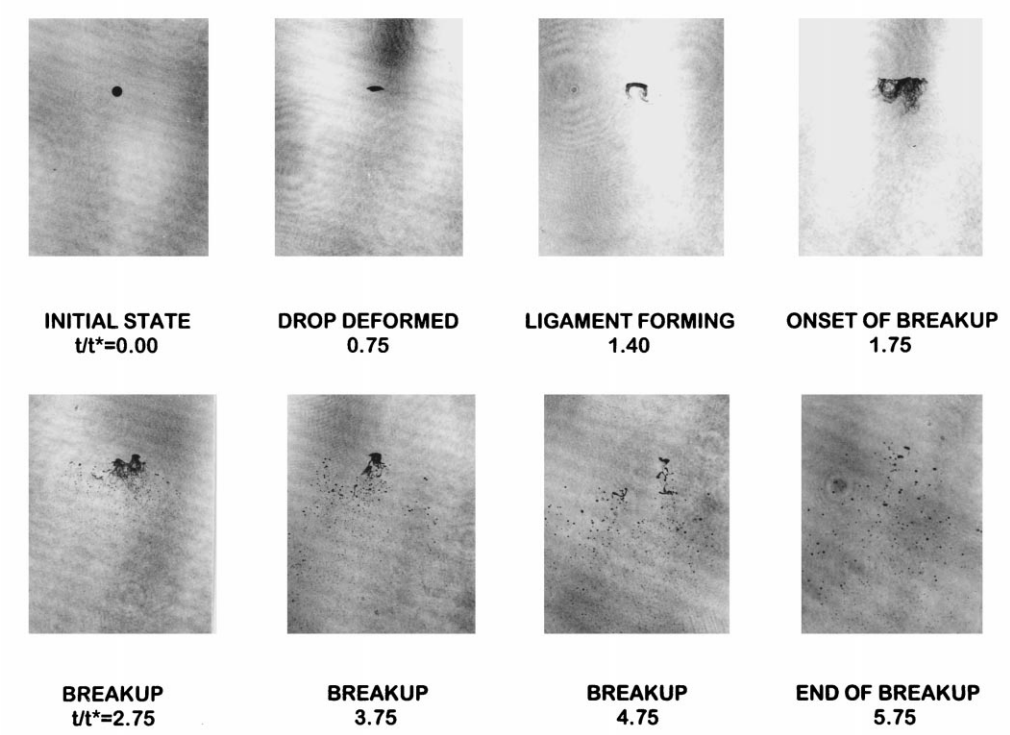

Fig. 7. Pulse shadowgraphs of secondary breakup in the shear breakup regime (ethyl alcohol, $We = 81$, $Oh = 0.0126$).

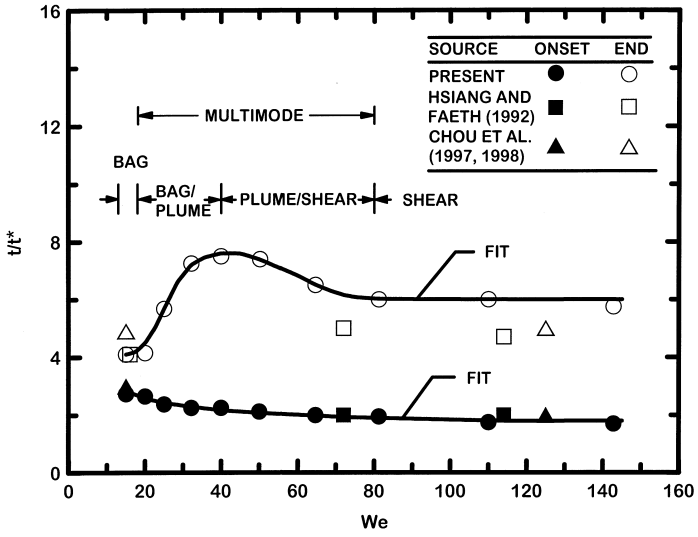

Fig. 8. Times of onset and end of breakup as a function of *We*. Measurements of Hsiang and Faeth (1992), Chou et al. (1997), Chou and Faeth (1998) and the present investigation.

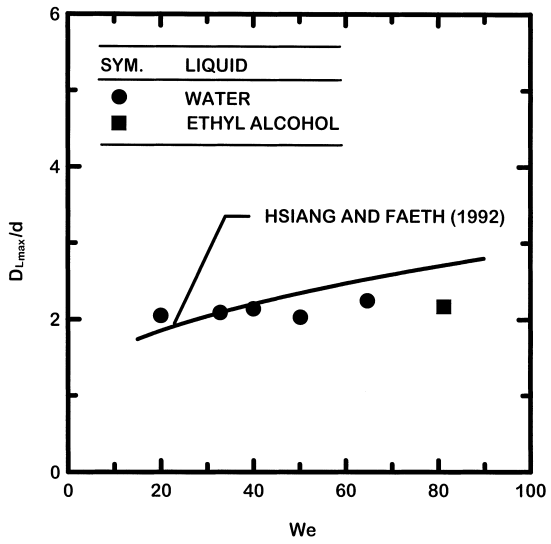

Fig. 9. Maximum cross stream dimension of the drop at the onset of breakup. Measurements of Hsiang and Faeth (1992) and the present investigation.

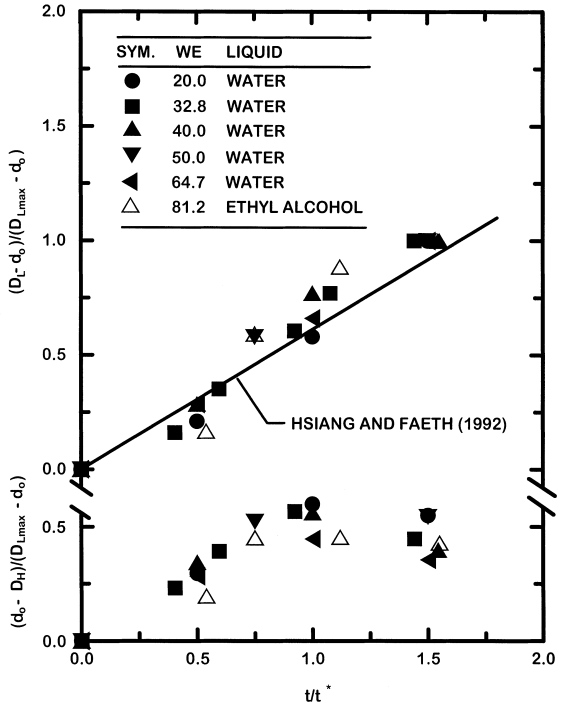

Fig. 10. Evolution of drop deformation as a function of time prior to the onset of breakup. Measurements of Hsiang and Faeth (1992) and the present investigation.

for We of 4–21, those of Engel (1958) for We of 10^3–10^4, those of Ranger and Nicholls (1969) for We of 10^3–10^5, and those of Wierzba and Takayama (1988) for We of 10^2–10^4. There is a tendency for the measurements at large Weber numbers, $We > 10^2$, to be consistently above the correlation of Hsiang and Faeth (1992) and another expression probably should be used for these results. Present measurements, however, are in good agreement with those of Hsiang and Faeth (1992) at comparable Weber numbers and can be correlated quite well by their expression.

3.4. Drop drag coefficient

Similar to past work by Hsiang and Faeth (1992), the drop/drag coefficient is defined in terms of the local relative velocity, $u_\infty - u_p$, where u_∞ is the local gas velocity and u_p is the local drop velocity, and the cross stream dimensions of the drop, as follows:

$$C_D = D/\left(\pi\rho_G D_L^2(u_\infty - u_p)^2/8\right) \tag{2}$$

where D is the local drag force on the drop. Drop/drag properties were found by measuring the motion of the centroid of the drop in the uniform flow field behind the shock wave. This approach is only approximate because it neglects redistribution of drop mass due to deformation but the error is small because liquid velocities are small, of the order of 1% of the initial relative velocity. In addition, pressure gradient forces were neglected because the flow behind the shock wave was uniform and virtual mass and Basset history forces were neglected because $\rho_L/\rho_G \gg 1$. The final formulation used to compute C_D under these assumptions can be found in Hsiang and Faeth (1992); the experimental uncertainties (95% confidence) in present

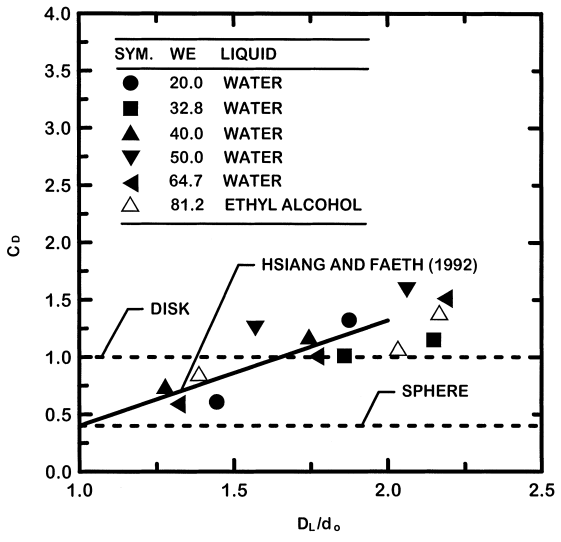

Fig. 11. Evolution of drop/drag coefficient as a function of time period prior to the onset of breakup. Measurements of Hsiang and Faeth (1992) and the present investigation.

determinations of C_D are less than 30%, mainly governed by uncertainties in locating the centroid of the deforming drops.

The experiments to find C_D involved the deformation period of the drops prior to the onset of breakup, $Oh < 0.1$ and Re of 1000–3300 (counting data drawn from earlier studies) where effects of Re on drop drag are expected to be small (White, 1974). Thus, C_D was largely a function of degree of deformation of the drop, D_L/d_0, and is correlated in this manner following Hsiang and Faeth (1992), as illustrated in Fig. 11. Measurements of C_D for solid spheres and thin disks, drawn from White (1974) at comparable Re, as well as an earlier correlation of measurements of Hsiang and Faeth (1992) for similar conditions as the present investigation, are also shown in the plot. Present measurements agree very well with the results of Hsiang and Faeth (1992). Quite plausibly, the results exhibit transition from findings similar to round spheres for $D_L/d_0 \approx 1$ to results typical of thin disks for $D_L/d_f \approx 2$. Combined with the increase of the cross stream diameter of the drop, the results of Figs. 9 and 11 indicate that drop/drag forces increase by a factor of roughly 16 between the start and end of the drop deformation period, with the corresponding rapid increase of drop acceleration providing ample reason for the onset of drop breakup.

3.5. Volume fractions of bag, ring, plume and core drops

The volume fractions of the bag, ring, plume and core drops are plotted as a function of the Weber number in Fig. 12, for $Oh < 0.1$. The volume of the ring was determined similarly to Chou and Faeth (1998) for bag breakup, from the dimensions of the ring at the end of breakup of the bag. The plume also had a reasonably regular shape so that its volume was

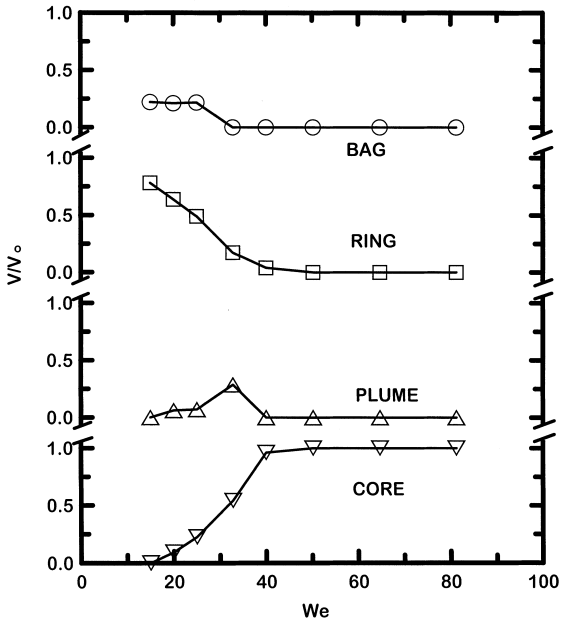

Fig. 12. Volumes of the bag, ring, plume and core drops as a function of We.

computed from its projected image assuming that it had a round cross section. The volume of the core drop was found by measuring the sizes of all drops formed from the core drop and summing their volumes; this approach was required because the core drop was rather irregular in shape for $We > 33$. Finally, the volume of the bag drops was found by difference, given the initial drop volume and the volume of the ring, plume and core drops. Experimental uncertainties in the maximum volumes of the ring and plume drops (95% confidence) are less than 10% at their maximum volume conditions, increasing inversely proportional to volume for smaller volumes. The uncertainties for the core drop at volume fractions less than 80% are comparable to the ring and plume drops with this uncertainty becoming negligible for $We > 40$, where all the drops originate from the core drop, similar to the shear breakup regime.

The results plotted in Fig. 12 at a value of $We = 15$ imply 75% of the drop volume in the ring, 25% in the bag and negligible volumes associated with the plume and the core. This finding is in good agreement with an early determination of ring volume due to Lane (1951) who also finds 75% of the volume associated with the ring at this condition. On the other hand, Chou and Faeth (1998) find 56% of the drop volume associated with the ring and 44% with the bag at this condition; unfortunately, repeated testing was unable to resolve the discrepancy. The volume of the bag and the ring progressively decrease with increasing We; with both elements finally disappearing at $We = 40$, where the bag/plume breakup regime ends. Over the same We range, the liquid volume fraction in the plume increases at first to reach a maximum of 25% at $We = 33$ and then decreases to zero once again at $We = 40$. The volume fraction of the core drop also progressively increases with increasing We within the bag/plume regime and then remains constant at 100% in the plume/shear breakup regime for $We > 40$.

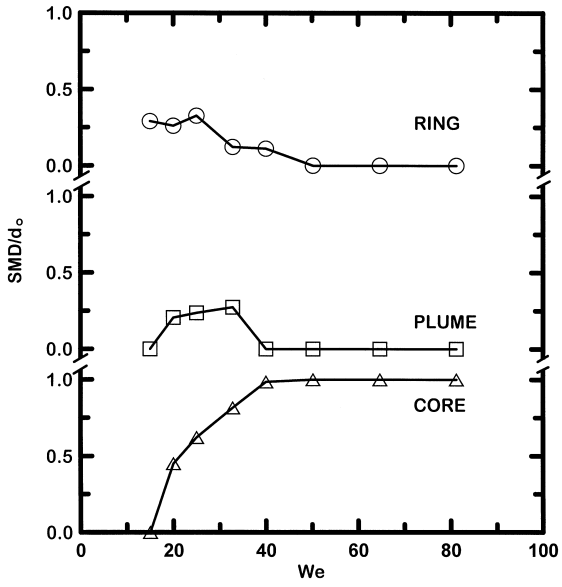

Fig. 13. SMD of the ring, plume and core drops as a function of We.

3.6. Sizes of ring, plume and core drops

The sizes of the ring, plume and core drops are plotted as a function of We in Fig. 13 for $Oh < 0.1$. These sizes are given by SMD/d_0, with each of these drop groups best treated as being approximately monodisperse. The sizes of bag drops were small and were not resolved during the present measurements; the results of Chou and Faeth (1998) for bag breakup suggest SMD/d_0 of 3–5% and the present bag drops were either comparable to or smaller than these sizes. At $We = 15$ in the bag breakup regime, $SMD/d_0 \approx 0.27$ which agrees with the measurements of Chou and Faeth (1998) at these conditions. The size of the ring drops progressively decreases with increasing We, however, reaching zero at $We = 40$ which corresponds to the end of the bag/plume breakup regime. The SMD of plume drops increases with increasing We in the bag/plume region for a time, reaching a maximum of $SMD/d_0 = 0.30$ at $We = 33$ where the volume of the plume reaches a maximum as well. Plume drop sizes subsequently decrease, reaching zero at $We = 40$ which corresponds to the end of the bag/plume regime. Thus, the maximum sizes of the ring and the plume drops are roughly the same. However, the number of ring drops is much larger than the number of plume drops (which is typically near ten for a single drop breakup) due to the larger volume fractions of the ring at small We (see Fig. 12). The core drop first appears at the onset of the bag/plume breakup regime and progressively increases in size with increasing We in this regime; by definition, however, $SMD/d_0 = 1$ for the core drop in the plume-shear breakup regime for $We > 40$.

3.7. Velocities of parent and post breakup drops

The velocities of parent and post breakup drops, u_p and u, are plotted as a function of normalized time in Fig. 14. Chou and Faeth (1998) present simplified analysis that proves to be

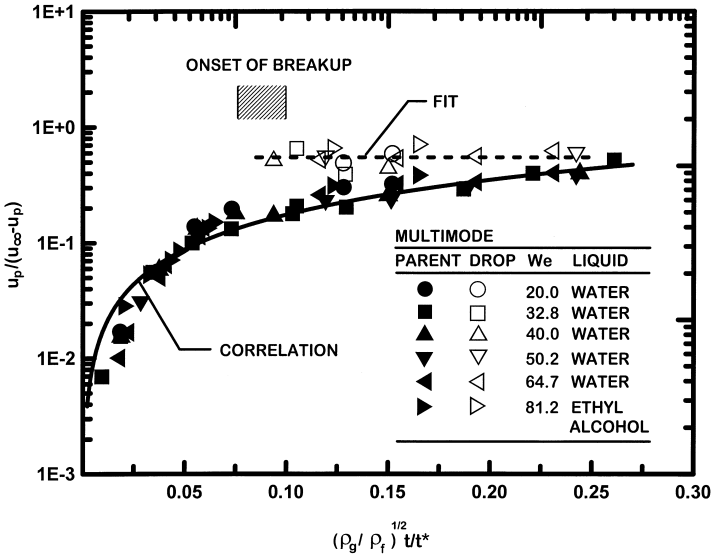

Fig. 14. Velocities of parent and post breakup drops as a function of time during breakup.

helpful in correlating drop velocities. The parent drop velocities for bag breakup from Chou and Faeth (1998) and the present times of onset of breakup, are plotted in Fig. 14 for reference purposes, based on the Chou and Faeth (1998) analysis. For this figure, the parent drop is defined as all the liquid that will continue to break up as time increases. Before the onset of breakup, the parent drop velocity is taken to be the velocity of the centroid of the entire drop. After the onset of breakup, the parent drop velocity is taken to be the velocity of the leading edge of the parent drop. Similar to past observations of bag and shear breakup (Chou and Faeth 1998; Hsiang and Faeth 1992, 1993, 1995), the parent drop exhibits considerable acceleration during the breakup period, due to the growth of the cross stream dimensions of the deformed parent drop as a result of deformation and bag formation. The acceleration decreases during the latter stages of breakup because cross stream dimensions decrease once again. Near the onset of breakup, however, the velocities of post breakup drops are larger than the parent drop because these drops are small and tend to accommodate to the gas velocity sooner than the parent drop. Similar to the observations of Chou and Faeth (1998) in the bag breakup regime, the absolute and relative velocities of the parent drop, u_p and $u_\infty - u_p$, tend to be comparable, which implies a reduction in the relative velocity of the parent drop by roughly 50% during the time of breakup, which is quite substantial.

3.8. Volume removal rates from the parent drop

Present measurements of the cumulative volume percentage of liquid removed from the parent drop are plotted in Fig. 15 as a function of normalized time. Correlations also shown in the plot include results for shear breakup due to Chou et al. (1997); results for bag breakup due to Chou and Faeth (1998) and a correlation taken as the mean of present measurements of multimode breakup. The results for bag breakup exhibit step-like changes due to rapid

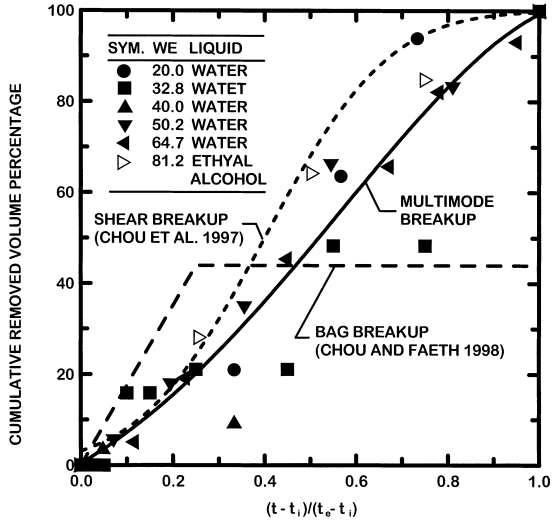

Fig. 15. Cumulative volume removed from the parent drop as a function of time during breakup. Measurements of Chou et al. (1997), Chou and Faeth (1998) and the present investigation.

breakup of bag drops and nearly simultaneous breakup of ring drops, see Chou and Faeth (1998). Results for shear breakup are more continuous due to the stripping of drops from the parent drop, see Chou et al. (1997). Present results for multimode breakup are intermediate between the behaviors of the bag and shear breakup processes, which is quite reasonable. The differences between these limits, however, show that it is impossible for behavior during the multimode breakup to collapse to a single curve. Nevertheless, the correlation shown in the figure should still be useful for modeling and simulating spray structure.

4. Conclusions

The present investigation considered the temporal properties of secondary drop breakup due to shock-wave disturbances in the multimode breakup regime for $Oh < 0.1$; see Table 1 for a detailed specification of the present test range. The major conclusions of the study are as follows:

1. With increasing Weber numbers, the multimode breakup regime begins at the end of the bag breakup regime at $We = 18$ and ends at the start of the shear breakup regime at $We = 80$. The multimode breakup regime can be subdivided into a bag/plume breakup regime for $We = 18$–40 and a plume/shear breakup regime for $We = 40$–80 with the transition between these regimes fixed by the disappearance of bag and ring structures and the attainment of a maximum breakup time.
2. With increasing We in the range 18–80, t/t^* at the onset of breakup decreases from a value of 3.0 to a value of 2.0 at the onset of shear breakup. The end of breakup has values of $t/t^* = 4.0$ and 5.0 at the end of bag breakup and the beginning of shear breakup but reaches a maximum value of t/t^* of 7.5 at the transition between the bag/plume and plume/shear regimes at $We = 40$ because Rayleigh breakup of the plume is slow.
3. Drop deformation and drag properties prior to the onset of breakup appear to be relatively universal for We of 13–150. The drop/drag coefficient transitions from values similar to spheres to values similar to thin disks as the cross stream dimension of the drop D_{Lmax}/d_0 varies in the range 1.0–2.0 and the onset of breakup is approached. These two effects cause drop/drag forces to increase 16:1 in the deformation period for present test conditions, with associated drop accelerations leading to breakup onset.
4. Liquid volume fractions associated with the bag, ring, plume and core drops have been found for We of 18–80, and the sizes of ring, plume, and core drops have been found for the same range of conditions. The sizes of drops formed by breakup of the bag and the core drops were not found but should approximate the known behavior in the bag and shear breakup regimes until specific information becomes available. The velocities of the parent drop were similar to behavior observed by Chou and Faeth (1998) for bag breakup, whereas, the velocities of post breakup drops exhibited continuous variations with increasing t/t^* and did not indicate any sudden changes at transitions to new breakup regimes.
5. The mass removal rates of liquid from the parent drop resembles behavior in the bag breakup regime at small We and behavior in the shear breakup regime at large We. The differences between these behaviors are not large compared to experimental uncertainties,

however, yielding a reasonable correlation of liquid removal rates for spray modeling purposes.

Acknowledgements

This research was sponsored by the Air Force Office of Scientific Research Grant Nos. F49620-95-1-0364 and F49620-99-1-0083, under the technical management of J.M. Tishkoff. The authors would like to thank C.W. Kauffman for the loan of the shock tube facility and advice concerning its operation. The U.S. Government is authorized to reproduce and distribute copies of this article for governmental purposes notwithstanding any copyright notation thereon.

References

Chou, W.-H., Faeth, G.M., 1998. Temporal properties of secondary drop breakup in the bag breakup regime. Int. J. Multiphase Flow 24, 889–912.

Chou, W.-H., Hsiang, L.-P., Faeth, G.M., 1998. Temporal properties of drop breakup in the shear breakup regime. Int. J. Multiphase Flow 23, 651–669.

Clift, R., Grace, J.R., Weber, M.E., 1978. Bubbles, Drops and Particles, 26. Academic Press, New York, pp. 339–347.

Dabora, E.K., 1967. Production of monodisperse sprays. Rev. Sci. Instru 38, 502–506.

Engel, O.G., 1958. Fragmentation of waterdrops in the zone behind an air shock. J. Res. Natl. Bur. Stds 60, 245–280.

Faeth, G.M., 1990. Structure and atomization properties of dense turbulent sprays. In: Twenty-Third Symposium (International) on Combustion. The Combustion Institute, Pittsburgh, 1345–1352.

Faeth, G.M., 1996. Spray combustion phenomena. In: Twenty-Sixth Symposium (International) on Combustion. The Combustion Institute, Pittsburgh, 1593–1612.

Gel'fand, B.E., 1996. Droplet breakup phenomena in flows with velocity lag. Prog. Energy Combust. Sci. 22, 201–265.

Giffen, E., Muraszew, A., 1953. The Atomization of Liquid Fuels. Chapman & Hall, London.

Hassler, G., 1970. Breakup of large water drops under the influence of aerodynamic forces in a steady stream of steam at subsonic velocity. In: Third International Conference on Rain Erosion and Related Phenomena, Hampshire, England.

Hinze, J.O., 1955. Fundamentals of the hydrodynamic mechanism of splitting in dispersion processes. AIChE. J. 1, 289–295.

Hsiang, L.-P., Faeth, G.M., 1992. Near-limit drop deformation and secondary breakup. Int. J. Multiphase Flow 18, 635–652.

Hsiang, L.-P., Faeth, G.M., 1993. Drop properties after secondary breakup. Int. J. Multiphase Flow 19, 721–735.

Hsiang, L.-P., Faeth, G.M., 1995. Drop deformation and breakup due to shock wave and steady disturbances. Int. J. Multiphase Flow 21, 545–560.

Krzeczkowski, S.A., 1980. Measurements of liquid droplet disintegration mechanism. Int. J. Multiphase Flow 6, 227–239.

Lane, W.R., 1951. Shatter of drops in streams of air. Ind. Engr. Chem. 43, 1312 and 1317.

Lange, N.A., 1952. Handbook of Chemistry, 8th ed. Handbook Publishers, Sandusky, OH. pp. 1134 and 1709.

Liang, P.Y., Eastes, T.W., Gharakhari, A. 1988. Computer simulations of drop deformation and drop breakup. AIAA Paper No. 88-3142.

Ranger, A.A., Nicholls, J.A., 1969. The aerodynamic shattering of liquid drops. AIAA J. 7, 285–290.

Sangiovanni, J., Kestin, A.S., 1977. A theoretical and experimental investigation of the ignition of fuel droplets. Combust. Sci. Tech. 6, 59–70.

White, F.M., 1974. Viscous Fluid Flow. McGraw-Hill, New York.

Wierzba, A., Takayama, K., 1987. Experimental investigation on liquid droplet breakup in a gas stream. Rept. Inst. High Speed Mech. (Tohoku Univ.) 53 (382), 1–99.

Wierzba, A., Takayama, K., 1988. Experimental investigation of the aerodynamic breakup of liquid drops. AIAA J. 26, 1329–1335.

Wu, P.-K., Hsiang, L.-P., Faeth, G.M., 1995. Aerodynamic effects on primary and secondary breakup. Prog. Astro. Aero. 169, 247–279.